What we can learn from molecular spectroscopy of astronomical sources

David Neufeld
Johns Hopkins University

Outline

1. Introduction: Our Molecular Universe

2. The interaction of molecules with radiation: the physics of electronic, vibrational, and rotational transitions

3. Astronomical instrumentation for the mid-infrared, and the unique capabilities of EXES

4. Examples of mid-IR spectra, and the wealth of information they provide when interpreted carefully

Molecules are ubiquitous

A wide variety of molecules are found in a wide variety of astrophysical environments:

Interstellar medium – sites of star formation
Circumstellar outflows (from evolved stars)
Cometary comae
Accretion disks (protostellar/protoplanetary, AGN)
High-z galaxies
Stellar and planetary atmospheres

List of ~ 250 molecules detected in the ISM: some familiar, some very exotic

Roughly 250 molecules have now been detected in interstellar and circumstellar gas

Cologne Database for Molecular Spectroscopy (CDMS) list of interstellar and circumstellar molecules

2 atoms		3 atoms				6 atoms		9 atoms	11 atoms
H_2	O_2	C_3 *	HCP	HNCS	CH_4 *	C_5H	CH_3NCO	CH_3C_4H	HC_9N
AlF	CF^+	C_2H	CCP	$HOCO^+$	HC_3N	l-H_2C4	$HOCH_2CN$	CH_3CH_2CN	CH_3C_6H
AlCl	SiH ?	C_2O	AlOH	H_2CO	HC_2NC	C_2H_4*	HCCCHNH	$(CH_3)_2O$	C_2H_5OCHO
C_2**	PO	C_2S	H_2O^+	H_2CN	HCOOH	CH_3CN	HC_4NC	CH_3CH_2OH	$CH_3OC(O)CH_3$
CH	AlO	CH_2	H_2Cl^+	H_2CS	H_2C_2O	CH_3NC	c-C_3HCCH	HC_7N	CH3C(O)CH_2OH
CH^+	OH^+	HCN	KCN	H_3O^+	H_2NCN	CH_3OH	MgC_5N	C_8H	c-C_5H_6
CN	CN^-	HCO	FeCN	c-SiC_3	HNC_3	CH_3SH	l-H_2C_5	$CH_3C(O)NH_2$	$HOCH_2CH_2NH_2$
CO	SH^+	HCO^+	HO_2	CH_3 *	SiH_4 *	HC_3NH^+	CH2C3N	C_8H^-	
CO^+	SH	HCS^+	TiO_2	C_3N–	H_2COH^+	HC_2CHO		C_3H_6	12 atoms
CP	HCl^+	HOC^+	C_2N	PH_3	C_4H^-	NH_2CHO	8 atoms	CH_3CH_2SH	c-C_6H_6 *
SiC	TiO	H_2O	Si_2C	HCNO	HC(O)CN	C_5N	CH_3C_3N	CH_3NHCHO	n-C_3H_7CN
HCl	ArH^+	H_2S	HS_2	HOCN	HNCNH	l-HC_4H *	$HC(O)OCH_3$	HC_7O	i-C_3H_7CN
KCl	NO^+ ?	HNC	HCS	HSCN	CH_3O	l-HC_4N	CH_3COOH	HCCCHCHCN	$C_2H_5OCH_3$
NH	NS^+	HNO	HSC	H_2O_2	NH_4^+	c-H_2C_3O	C_7H	H_2CCHC_3N	1-c-C_5H_5CN
NO	HeH^+	MgCN	NCO	C_3H^+	H_2NCO^+	H_2CCNH ?	C_6H_2	$H_2CCCHCCH$	2-c-C_5H_5CN
NS		MgNC	CaNC	HMgNC	$NCCNH^+$	C_5N^-	CH_2OHCHO		
NaCl		N_2H^+	NCS	HCCO	CH_3Cl	HNCHCN	l-HC_6H *	10 atoms	> 12 atoms
OH		N_2O	4 atoms	MgC_2H	MgC_3N		CH_2CHCHO	CH_3C_5N	C_{60} *
PN		NaCN	c-C_3H	HCCS	NH_2OH	7 atoms	CH_2CCHCN	$(CH_3)_2CO$	C_{70} *
SO		OCS	l-C_3H	HNCN	HC_3O+	C_6H	H_2NCH_2CN	$(CH_2OH)_2$	C_{60}^+ *
SO^+		SO_2	C_3N	H_2NC	HC_3S+	CH_2CHCN	CH_3CHNH	CH_3CH_2CHO	c-C_6H_5CN
SiN		c-SiC_2	C_3O		H_2C_2S	CH_3C_2H	CH_3SiH_3	CH_3CHCH_2O	$HC_{11}N$
SiO		CO_2 *	C_3S	5 atoms	C_4S	HC_5N	$H_2NC(O)NH_2$	CH_3OCH_2OH	1-$C_{10}H_7CN$
SiS		NH_2	C_2H_2*	C_5 *	HC(O)SH	CH_3CHO	$HCCCH_2CN$	c-C_6H_4	2-$C_{10}H_7CN$
CS		H_3^+ (*)	NH_3	C_4H	HC(S)CN	CH_3NH_2	HC_5NH^+	H_2CCCHC_3N	c-C_9H_8
HF		SiCN	HCCN	C_4Si		c-C_2H_4O	CH_2CHCCH	C_2H_5NCO	1-c-C_5H_5CCH
HD		AlNC	$HCNH^+$	l-C_3H_2		H_2CCHOH	MgC_6H		2-c-C_5H_5CCH
FeO ?		SiNC	HNCO	c-C_3H_2		C_6H^-	$C_2H_3NH_2$		
				H_2CCN					

*vibrational spectra only **electronic spectra only (updated Nov. 2021)

Molecules as probes and coolants

Molecules are valuable as probes of the environment in which they are detected, providing unique information about

a) excitation conditions: thanks to the rich spectrum of rotational, vibrational and electronic transitions
b) gas kinematics: thanks to the high spectral resolution that is achievable
c) cosmic rays and UV radiation, which affect the chemical composition
d) isotopic abundances: thanks to the large isotopic shift
e) magnetic fields: thanks to the Zeeman shift

Molecular emissions can dominate the cooling

a) in molecular clouds
b) in circumstellar envelopes
c) in the early Universe, where H_2 was present prior to the existence of heavy elements

Introduction: Our Molecular Universe

Carefully interpreted, observations of interstellar molecules can provide unique information of general astrophysical interest

The interpretation of such observations requires a detailed understanding of fundamental physical and chemical processes involved: “laboratory astrophysics”

The molecular astrophysics game plan

Laboratory astrophysics and related theory

Spectroscopy

Collisional excitation rate coefficients

Bimolecular reaction rate coefficients

Grain surface reactions

Photoionization and photodissociation cross-sections

Observations of astrophysical molecules

Emission line luminosities

Absorption line optical depths

Physical and chemical modeling of …

Diffuse interstellar clouds

Dense clouds

Photodissociation regions

Circumstellar outflows

X-irradiated regions

Excitation and radiative transfer

Interstellar shocks

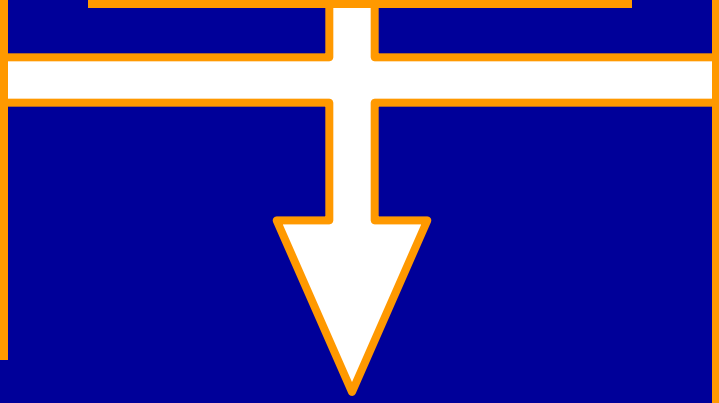

Information of general astrophysical interest

Interaction of molecules with radiation

Molecules can exist in a variety of quantum states: solutions to $H\psi = E\psi$

Transitions between these states can be accompanied by the absorption or emission of radiation

The different quantum states are characterized by different degrees of electronic excitation, vibration, and rotation

Potential energy curves for the H_2 molecule

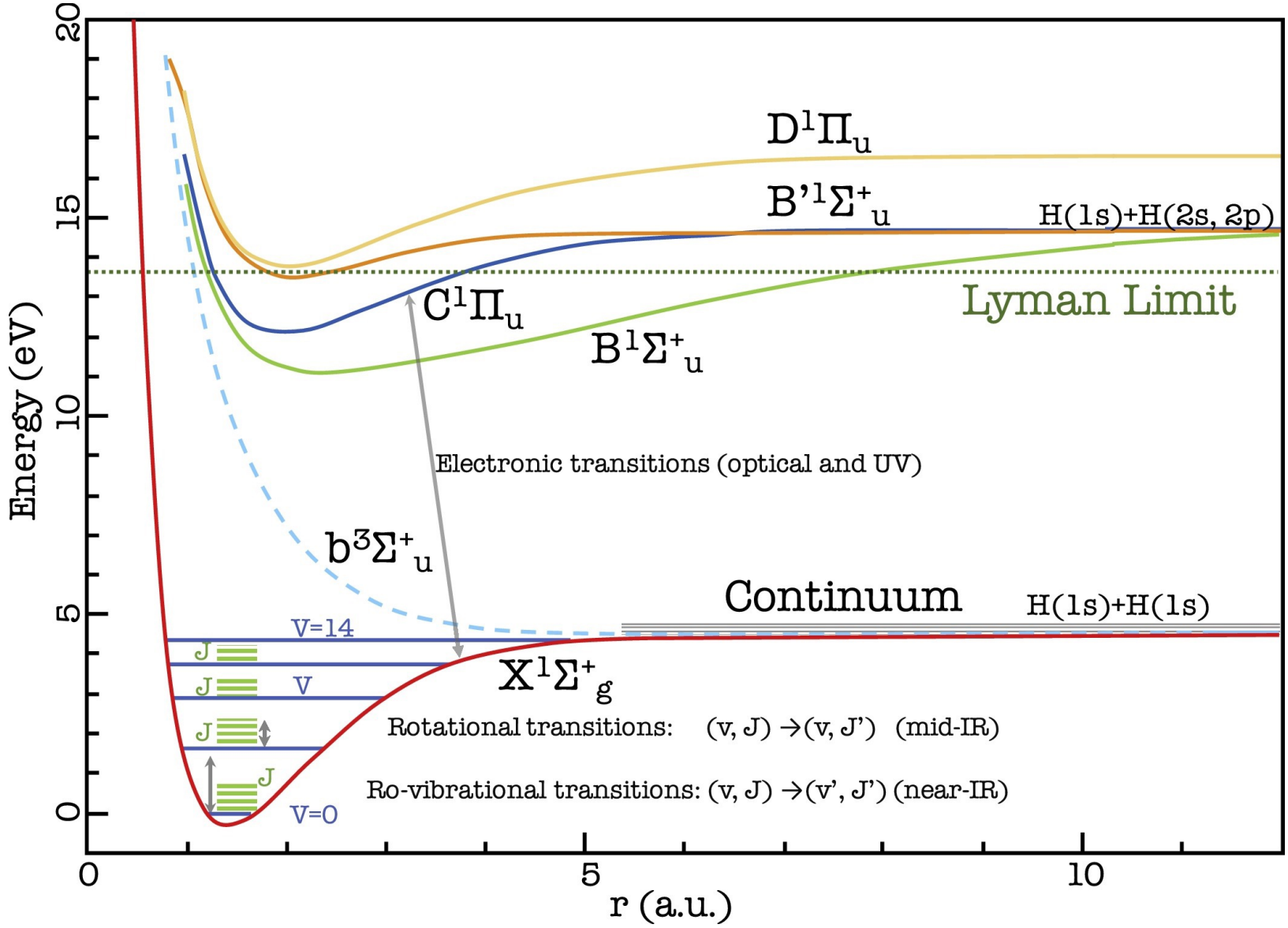

Figure from Wakelam et al.

The Born Oppenheimer approximation

Key realization: to very good approximation, the electron and nuclear motions can be treated separately

Particle momenta $p \sim \hbar/a_0$ for both nuclei and electrons

Electron velocities larger by a factor m_N/me ~ few x 10^3 – 10^5

Electron kinetic energies larger by the same factor

➔ initially neglect nuclear k.e. and assume that electronic wavefunction and k.e. energy responds instantly to slowly changing nuclear positions

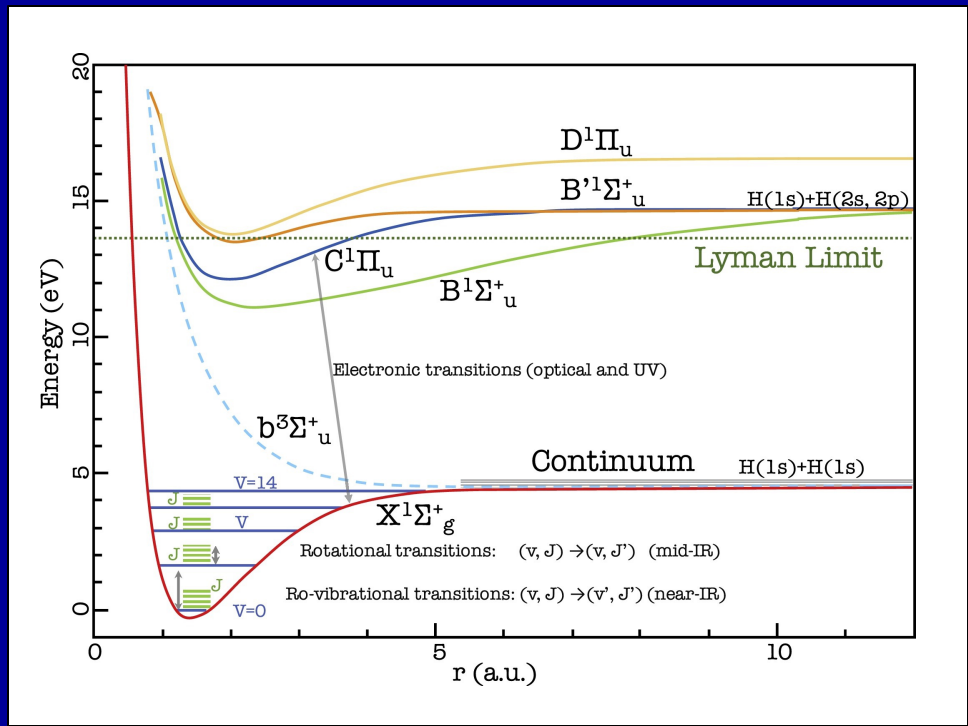

Characteristic length and energy scales

The characteristic length scale for atomic and molecular systems is the Bohr radius

$a_0 = \hbar^2/(m_e e^2) = 52.7$ pm (Recall $\psi_{H\,1s} \propto e^{-r/a_0}$)

The characteristic electronic energy is the Rydberg (binding energy of H 1s)

$E_{el} \sim e^2/2a_0 = e^4 m_e/(2\hbar^2) = \hbar^2/(2m_e {a_0}^2) = 13.6$ eV

Electronic transitions of molecules have typical energies ~ few eV and lie in the optical (CH, CH^+, CN) and ultraviolet (H_2, OH, H_2O, CO) with $\lambda \sim$ 1 – few $\times 10^{-1}\mu$m

Molecular rotation

Whatever the electronic state of a molecule, the entire molecule can also rotate. For a simple diatomic molecule

Rotational kinetic energy = $L^2/(2I)$ with

$L^2 = J(J+1)\,\hbar^2$ (square of angular momentum)

$I = \mu_N r^2$ (moment of inertia)

$\mu_N = m_{N1}m_{N2}/(m_{N1}+m_{N2})$ reduced mass of the nuclei

Rotational transitions in which *J* changes by 1 have characteristic energies $E_{rot} \sim J\hbar^2/(m_N a_0{}^2) \sim J(m_e/m_N)E_{el}$

With two heavy element nuclei (e.g. CO), the lowest rotational transitions have $E_{rot} \sim 10^{-4}\ E_{el} \sim$ few x 10^{-4} eV and lie in the millimeter spectral region with λ = 1 – few mm

With one heavy element nucleus (a hydride), the lowest energy rotational transitions have $E_{rot} \sim 10^{-3}\ E_{el} \sim$ few x 10^{-3} eV and λ = 1 – few x 100 μm (far-IR/submm region)

For H_2, the lowest rotational transition, *J* = 2 – 0, is at 28.3 μm

Molecular vibration

Molecules also have vibrational transitions. For a diatomic molecule, the vibrational energy is $(\mathrm{v} + 1/2)\hbar\omega_c$

where $\omega_c = \sqrt{k/\mu_N}$ is the classical frequency of oscillation for a spring constant k and v is an integer

This is related to the curvature of the potential energy curve at its minimum, since

$$E \sim E_0 + \tfrac{1}{2}\, k(R - R_0)^2$$

The spring constant is therefore of order $E_{el}/{a_0}^2 \sim (\hbar^2/mea_0{}^2)\ /{a_0}^2$

and thus $E_{vib} = \hbar\omega_c = \hbar\sqrt{k/\mu_N} = \hbar^2/[(m_e\mu_N)^{1/2}{a_0}^2] = E_{el}(m_e/\mu_N)^{1/2}$

For molecules with two heavy elements, the fundamental vibrational band (v = 1 – 0) has $E_{vib} \sim 10^{-2}\ E_{el} \sim$ few x 10^{-2} eV and lies in the mid-IR spectral region with $\lambda \sim$ few μm

Summary: electronic, vibrational and rotational transitions

A hierarchy of energy splittings is set by the proton-to-electron mass ratio (m_p/m_e = 1837)

$$E_{el} : E_{vib} : E_{rot} = 1 : (m_e/\mu_N)^{1/2} : (m_e/\mu_N)$$

yielding

1) Pure rotational transitions (in which the vibrational and electronic state remains constant). Examples

CO J = 1 – 0 at 2.6 mm (Ground)

CO J = 16 – 15 at 163 μm (GREAT)

H_2 J = 3 – 1 at 17.1 μm (EXES)

H_2 J = 5 – 3 at 12.3 μm (EXES)

2) Rovibrational transitions in which both the vibrational and rotational state change but the electronic state does not. Examples

CS v = 1 – 0 band near 7.8 μm (EXES)

H_2O v_2 = 1 – 0 band near 6.0 μm (EXES)

NH_3 v_2 = 1 – 0 band near 13.7 μm (EXES)

HCN v_2 = 2 – 0 band near 14.0 μm (EXES)

3) Electronic transitions in which both the electronic, vibrational, rotational state all change. Examples

Lyman (B – X) and Werner (C – X) bands of H_2 in the vacuum UV (Copernicus, FUSE)

Potential energy curves for the H_2 molecule

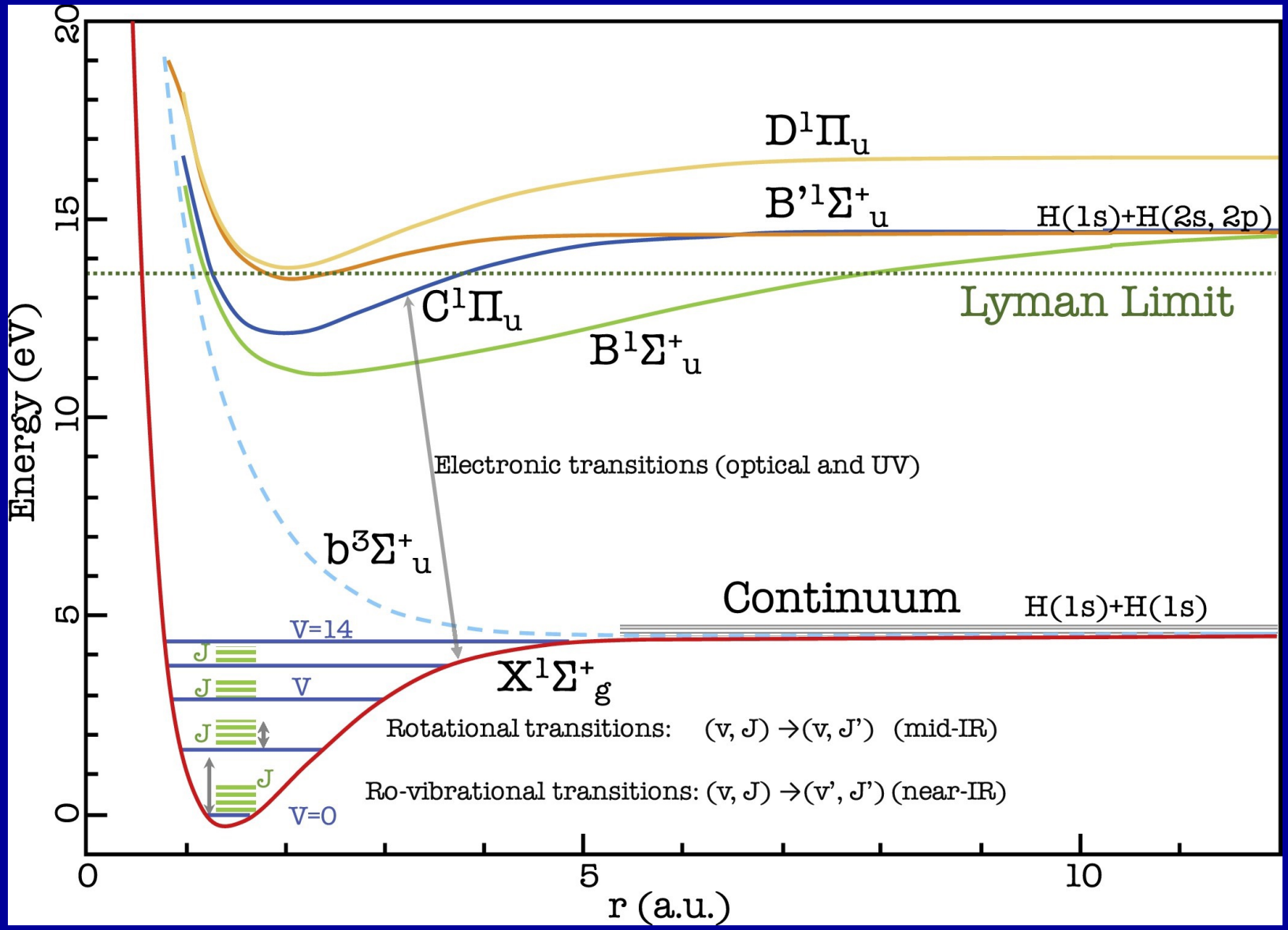

Figure from Wakelam et al.

Some nomenclature and notation

1) We specify electronic states with the notation R $^{2\Sigma+1}\Lambda_{Je,z}$

R is a roman letter than has no specific meaning except that the ground state is always called X

Σ is the projection of the total electron spin onto the internuclear axis

Λ is a capital Greek letter that specifies the projection of the total electronic orbital angular momentum Λ onto the internuclear axis. The code Σ, Π, Δ, Φ.. for $|\Lambda|$ = 0, 1, 2, 3 follows the s, p, d, f… convention for atomic electrons

$J_{e,z}$ is the projection of the total electronic angular momentum onto the internuclear axis

For homonuclear molecules, a subscripted *u* or *g* and superscripted + or – indicate the symmetry of the wavefunction

Some nomenclature and notation

2) For transitions we specify the rotational quantum numbers of the upper and lower state, J_L and J_U, with the notation $X(J_L)$ where

X takes the values O, P, Q, R, and S

for $J_U - J_L = -2, -1, 0, 1,$ and 2

Obviously, for pure rotational transitions we can only have R or S

For molecules with a dipole moment, the P, Q and R "branches" are strongly favored, except that Q is forbidden if both the upper and lower electronic states have $\Lambda = 0$ (i.e. are Σ states)

For molecules without a permanent dipole moment (e.g. H_2), only rovibrational transitions with O and S are permitted.

And a few more things

1) Polyatomic molecules (e.g. H_2O, HCN, NH_3)

a) Regarding the moments of inertia, there are 3 cases:

Linear molecule (e.g. HCN): $I_1 = I_2 \neq 0$, $I_3 = 0$ (like diatomic)
Symmetric top (e.g. NH_3): $0 \neq I_1 = I_2 \neq I_3 \neq 0$
Asymmetric top (e.g. H_2O) : I_1, I_2, I_3 all non-zero and different

For non-linear polyatomic molecules, the energy depends on both the total rotational angular momentum *and* its projection onto the principal axes of the molecule

b) There are also multiple vibrational modes (3 for a non-linear triatomic): e.g. bending, symmetric stretch, asymmetric stretch

And a few more things

2) Isotopic shifts

Key point: Unlike atoms, which lack rotational and vibrational modes of excitation, molecular line frequencies can show a strong dependence on nuclear mass. I wrote previously that $E_{el} \sim e^4 m_e/(2\hbar^2)$, but strictly I should have had $\mu_e = m_e m_N/(m_e + m_N) = m_e/(1 + m_e/m_N)$ in place of m_e. So there is some dependence on m_N but it's very weak because $m_N \gg m_e$. Even for D versus H, the fractional difference is only 3 x 10^{-4}.

But for vibrational transitions, $E_{vib} \propto \mu_N^{-1/2}$ and for rotational transitions $E_{rot} \propto \mu_N^{-1}$ ➔ much stronger dependence

If we can assume there is no "fractionation", e.g. $C^{18}O/C^{16}O = [^{18}O/^{16}O]$, then molecular observations can be a powerful probe of elemental isotopic abundances (providing information about nucleosynthetic history).

Or, if we are confident in the elemental abundances, some systems that exhibit fractionation can probe chemistry (e.g. CD/CH)

And a few more things

3) Nuclear spin

Many of the most abundant elements are "α-nuclei" with an even number of neutrons = number of protons. These are spinless (e.g. ^{4}He, ^{12}C, ^{16}O, ^{20}Ne, ^{24}Mg, ^{28}Si, ^{32}S, ^{36}Ar, ^{40}Ca)

But several abundant nuclei do have non-zero spin I (in parentheses):

^{1}H (½), ^{2}H (1), ^{14}N (1), ^{23}Na (3/2), ^{35}Cl (3/2), ^{37}Cl (3/2), ^{13}C (½)

(dominant isotopes in black, others in light blue)

If there is a non-zero electronic spin ($J \neq 0$), then the interaction leads to hyperfine splitting (e.g. in OH, which has $J = 1/2$), but this is generally negligible at the wavelengths and resoklving power of EXES

When there are two or more identical H nuclei, the total nuclear spin is correlated with the rotational state: the overall wavefunction must be antisymmetric with respect to interchange of the H nucleons (fermions)

Molecular data needs

Data needed to interpret molecular spectra include

(1) Wavelengths and transition rates

Key resources for the mid-IR: HITRAN (www.hitran.org)
Exomol (www.exomol.com)

(2) Collisional excitation rates

Key resources: Basecol (https://basecol.vamdc.eu)
Lamda (https://home.strw.leidenuniv.nl/~moldata/)

Further reading on molecular spectroscopy

Physics of the Interstellar and Intergalactic Medium,
by Bruce Draine (Princeton),
Chapter 5 (15 pages)

Microwave Spectroscopy ,
by Charles Townes and Arthur Schawlow (Dover, $16 e-book),
18 chapters (699 pages)

Astronomical instrumentation for mid-IR (3 – 30 μm) spectroscopy

		Instrument	λ/μm	Typical λ/Δλ	Type	SMA(1)	*D*/m	
Past missions		ISO/SWS	2.5 – 45 12 – 45	1500 30000	Grating F-P	1	0.6	Space
		Spitzer/IRS	5 – 39 10 – 37	100 600	Long-slit grating	32 5	0.85	Space (cold primary)
		SOFIA/EXES	5 – 28	up to 10^5	XD-echelle	6 – 60	2.5	Stratosphere
Currently operating								
	Space	JWST/MIRI	5 – 28	3000	IFU	900	6.5	Space
		JWST/NIRSPEC	0.6 – 5.3	2700	IFU	900	6.5	Space
	Ground	VLT/CRIRES	1 – 5(2)	10^5	XD-echelle	180	8.2	Paranal (Chile)
		IRTF/iShell	1 – 5(2)	80000	XD-echelle	30 –150	3.2	Maunakea (HI)
		Gemini/TEXES	5 – 25(2)	10^5	XD-echelle	15 – 36	8.1	Maunakea (HI)

(1) Spatial multiplex advantage
(2) Many gaps in coverage due to atmospheric absorption

Astronomical instrumentation for mid-IR (3 – 30 μm) spectroscopy

Most instruments (but not ISO/SWS) have 2D detector arrays that are used in various ways to achieve spectral and spatial multiplexing

Long-slit: disperse in one direction. The other direction gives the spatial variation along the slit

IFU (integral field unit): image slicer places light from each position within a 2D grid on the sky onto one row of the detector. The radiation is dispersed in the other direction.

Cross-dispersed echelle: light is dispersed at high resolution in one direction on the detector, with multiple orders separated in the other direction. Spatial information along the (relatively short) slit is also available.

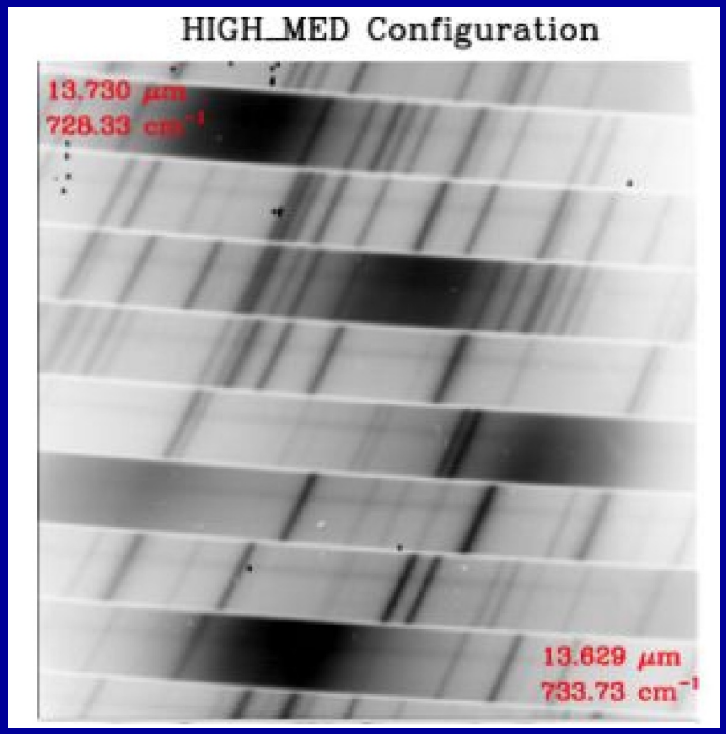

Example mid-IR spectra and what they reveal

Let's now look at two examples

Rotational emissions from H_2 in shocks

Vibrational absorption bands of H_2O observed towards hot cores

The Astrophysical Journal Letters, 878:L18 (7pp), 2019 June 10 https://doi.org/10.3847/2041-8213/ab2249

SOFIA/EXES Observations of Warm H_2 at High Spectral Resolution: Witnessing Para-to-ortho Conversion behind a Molecular Shock Wave in HH7

David A. Neufeld[1], Curtis DeWitt[2], Pierre Lesaffre[3,4], Sylvie Cabrit[4], Antoine Gusdorf[3,4], Le Ngoc Tram[2,5], and Matthew Richter[6]
[1] Department of Physics & Astronomy, Johns Hopkins University, Baltimore, MD 21218, USA
[2] SOFIA Science Center, NASA Ames Research Center, Moffett Field, CA 94035, USA
[3] Laboratoire de Physique de l'École normale supérieure, ENS, Université PSL, CNRS, Sorbonne Université, Université de Paris, France
[4] Observatoire de Paris, PSL University, Sorbonne Université, LERMA, 75014 Paris, France
[5] University of Science and Technology of Hanoi, VAST, Vietnam
[6] Universiy of California, Davis, CA 95616, USA
Received 2019 April 8; revised 2019 May 10; accepted 2019 May 17; published 2019 June 11

Abstract

Spectrally resolved observations of three pure rotational lines of H_2, conducted with the EXES instrument on SOFIA toward the classic bow shock HH7, reveal systematic velocity shifts between the S(5) line of ortho-H_2 and the two para-H_2 lines [S(4) and S(6)] lying immediately above and below it on the rotational ladder. These shifts, reported here for the first time, imply that we are witnessing the conversion of para-H_2 to ortho-H_2 within a shock wave driven by an outflow from a young stellar object. The observations are in good agreement with the predictions of models for nondissociative, C-type molecular shocks. They provide a clear demonstration of the chemical changes wrought by interstellar shock waves, in this case the conversion of para-H_2 to ortho-H_2 in reactive collisions with atomic hydrogen, and provide among the most compelling evidence yet obtained for C-type shocks in which the flow velocity changes continuously.

Key words: Herbig–Haro objects – infrared: ISM – ISM: molecules – molecular processes – shock waves

The Astrophysical Journal, 894:107 (21pp), 2020 May 10 https://doi.org/10.3847/1538-4357/ab88a1

The H_2O Spectrum of the Massive Protostar AFGL 2136 IRS 1 from 2 to 13 μm at High Resolution: Probing the Circumstellar Disk

Nick Indriolo[1], D. A. Neufeld[2], A. G. Barr[3], A. C. A. Boogert[4], C. N. DeWitt[5], A. Karska[6], E. J. Montiel[5], M. J. Richter[7], and A. G. G. M. Tielens[3]
[1] ALMA Project, National Astronomical Observatory of Japan, National Institutes of Natural Sciences, 2-21-1 Osawa, Mitaka, Tokyo 181-8588, Japan
[2] Department of Physics & Astronomy, Johns Hopkins University, Baltimore, MD 21218, USA
[3] Leiden Observatory, Leiden University, Leiden, The Netherlands
[4] Institute for Astronomy, University of Hawaii at Manoa, Honolulu, HI, 96822, USA
[5] USRA, SOFIA, NASA Ames Research Center MS 232-11, Moffett Field, CA 94035, USA
[6] Institute of Astronomy, Faculty of Physics, Astronomy and Informatics, Nicolaus Copernicus University, Grudziadzka 5, 87-100 Torun, Poland
[7] Department of Physics, University of California Davis, Davis, CA, 95616, USA
Received 2019 December 24; revised 2020 April 7; accepted 2020 April 10; published 2020 May 12

Abstract

We have observed the massive protostar AFGL 2136 IRS 1 in multiple wavelength windows in the near- to mid-infrared at high ($\sim$3 km s^{-1}) spectral resolution using VLT+CRIRES, SOFIA+EXES, and Gemini North +TEXES. There is an abundance of H_2O absorption lines from the ν_1 and ν_3 vibrational bands at 2.7 μm, from the ν_2 vibrational band at 6.1 μm, and from pure rotational transitions near 10–13 μm. Analysis of state-specific column densities derived from the resolved absorption features reveals that an isothermal absorbing slab model is incapable of explaining the relative depths of different absorption features. In particular, the strongest absorption features are much weaker than expected, indicating optical depth effects resulting from the absorbing gas being well mixed with the warm dust that serves as the "background" continuum source at all observed wavelengths. The velocity at which the strongest H_2O absorption occurs coincides with the velocity centroid along the minor axis of the compact disk in Keplerian rotation recently observed in H_2O emission with ALMA. We postulate that the warm regions of this dust disk dominate the continuum emission at near- to mid-infrared wavelengths, and that H_2O and several other molecules observed in absorption are probing this disk. Absorption line profiles are not symmetric, possibly indicating that the warm dust in the disk that produces the infrared continuum has a nonuniform distribution similar to the substructure observed in 1.3 mm continuum emission.

Unified Astronomy Thesaurus concepts: Massive stars (732); Water vapor (1791); Circumstellar disks (235)

H_2 rotational states

Absence of dipole moment ➔ $\Delta J = -2$ selection rule

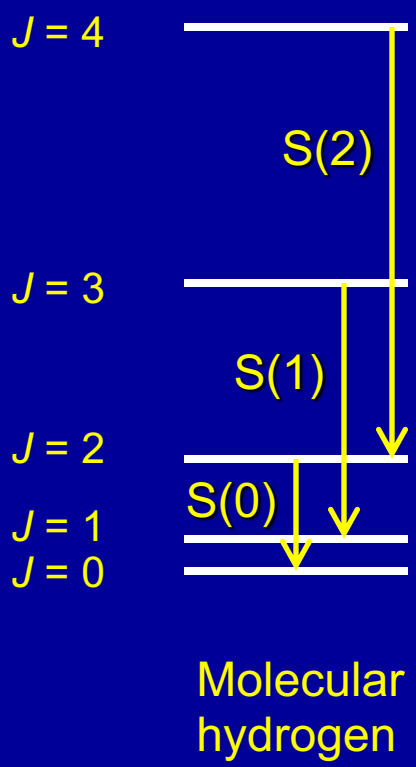

H_2 rotational states

The hydrogen nuclei are two identical spin-1/2 fermions

➔ wavefunction must be antisymmetric with respect to interchange of those nuclei

For the total spin = 1 state (ortho-H_2):

the rotational part of the wavefunction must be antisymmetric

➔ *J* is odd

For the total spin = 0 state (para-H_2):

the rotational part of the wavefunction must be symmetric

➔ *J* is even

H_2 rotational states

Absence of dipole moment ➔ $\Delta J = -2$ selection rule

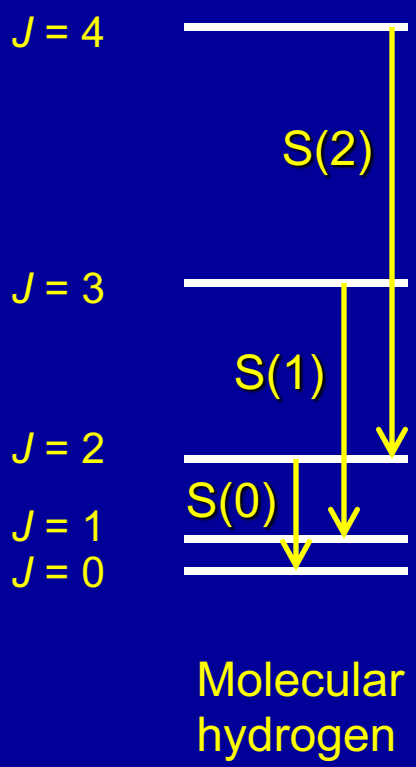

H_2 rotational states

Absence of dipole moment ➔ $\Delta J = -2$ selection rule

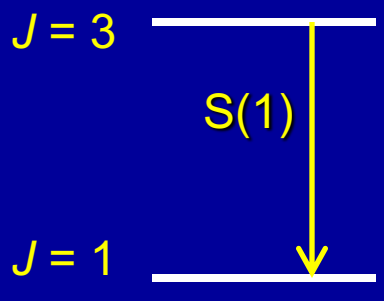

Ortho-hydrogen
Nuclear spin, $I = 1$

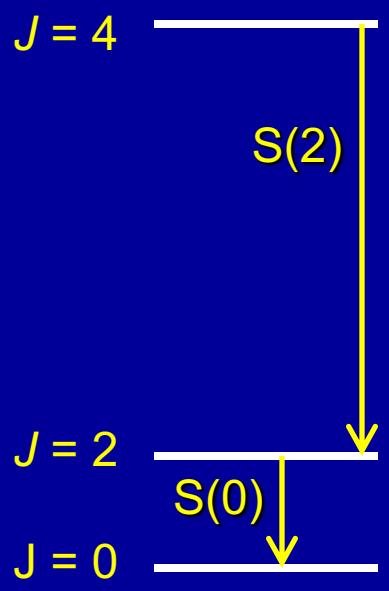

Para-hydrogen
Nuclear spin, $I = 0$

Ortho-to-para ratio in equilibrium

High temperature:

ortho-H_2/para-H_2 = 3, the ratio of the nuclear spin degeneracies

Low temperature:

Ortho-H_2/para-H_2 = $n_{J=1}$ / $n_{J=0}$

= 9 exp (–171 K /T)

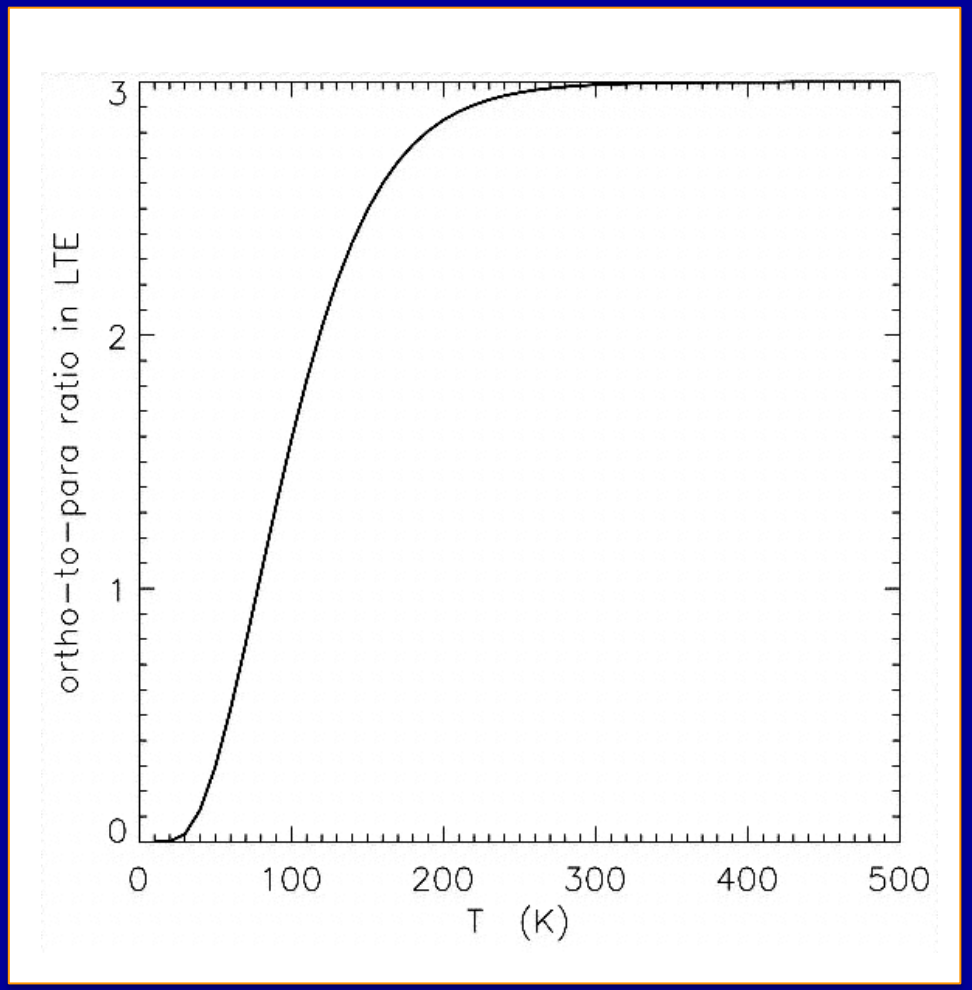

Ortho-para conversion is extremely slow

Not only are $\Delta J = \pm 1$ transitions radiatively forbidden, they are negligible in non-reactive inelastic collisions

Reason: a change from even → odd *J* must be accompanied by a change in nuclear spin

Implication: ortho-to-para conversion is very slow

A well known effect in the industrial production and storage of LH2

Straightforward refrigeration of H_2 leads to liquid H_2 with the ortho/para ratio initially "frozen in" at 3

Ortho-to-para ratio in equilibrium

Room temperature:

Ortho-H_2/para-H_2 = 3

LH2 temperature:

Ortho-H_2/para-H_2 = 0.01

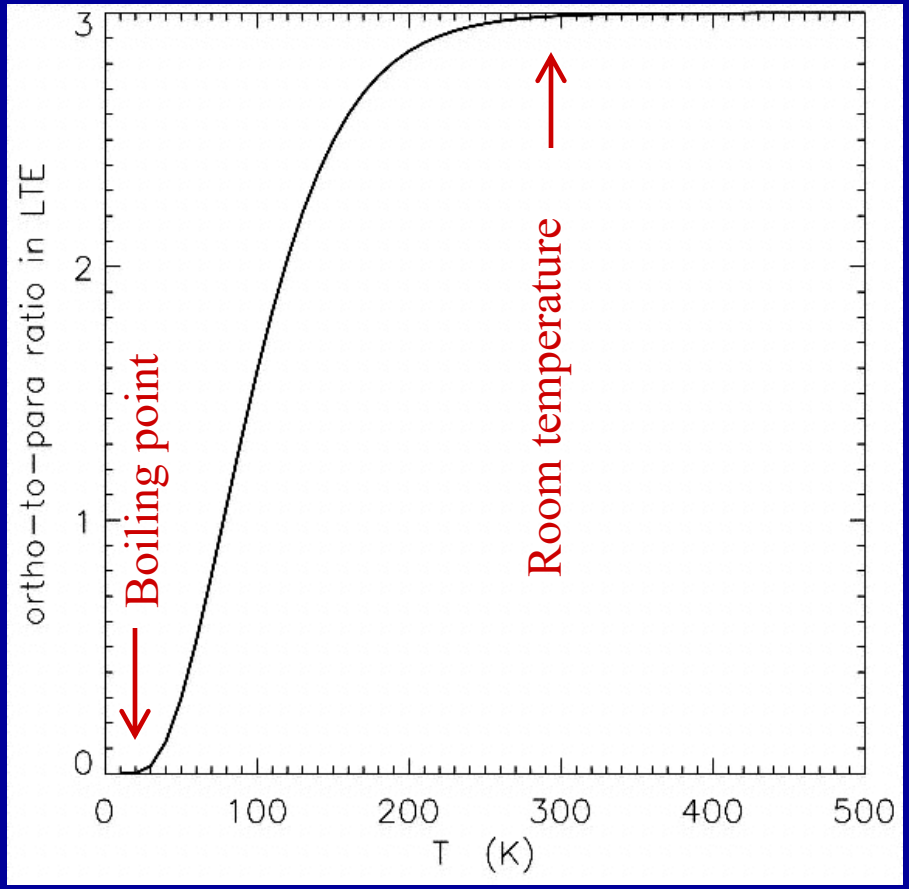

A well known effect in the industrial production and storage of LH2

Straightforward refrigeration of H_2 leads to liquid H_2 with the ortho/para ratio initially "frozen in" at 3

Ortho-para conversion proceeds slowly, with a timescale ~ 6.5 days, releasing heat as it occurs

A similar effect has also been observed with astrophysical H_2

Infrared Space Observatory (ISO/SWS) observations of HH54, a Herbig-Haro object in which molecular gas is shocked by a protostellar outflow

➔ detection of S(1) through S(5) pure rotational lines

(Neufeld et al. 1998, ApJL)

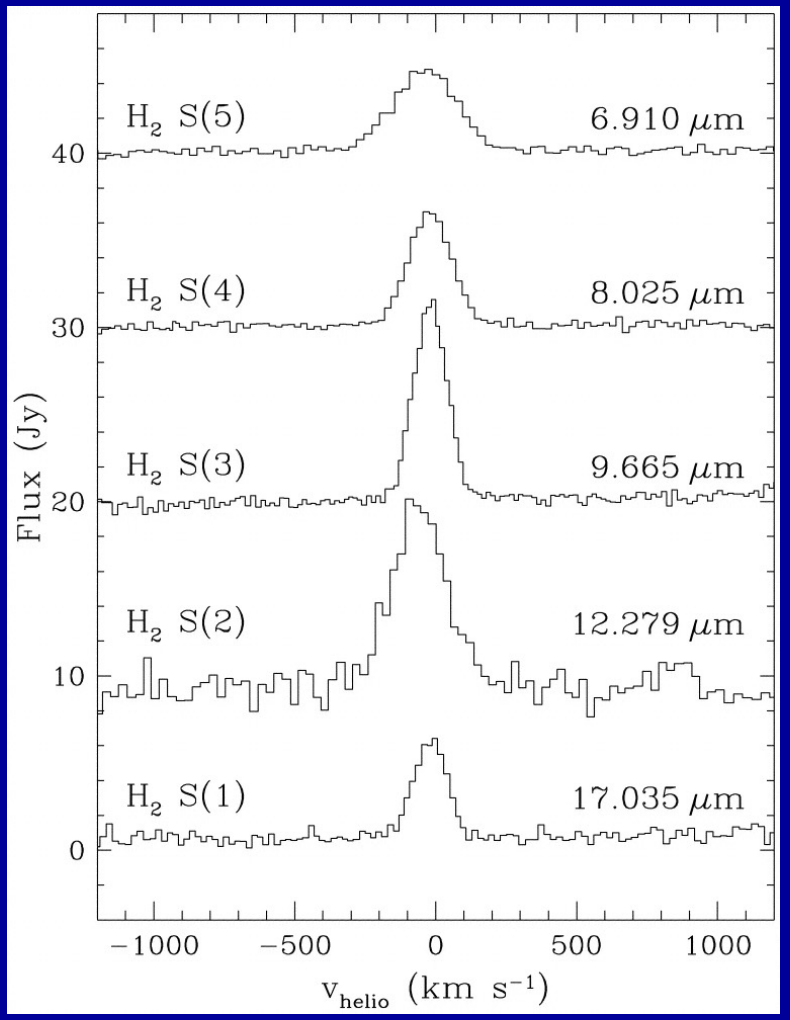

HH54 rotational diagram

Zigzag behavior

➔ ortho-para ratio out of equilibrium

Slope ➔ T_{gas} = 650 K

Ortho-para ratio = 1.2

➔ T_{op} = 90 K

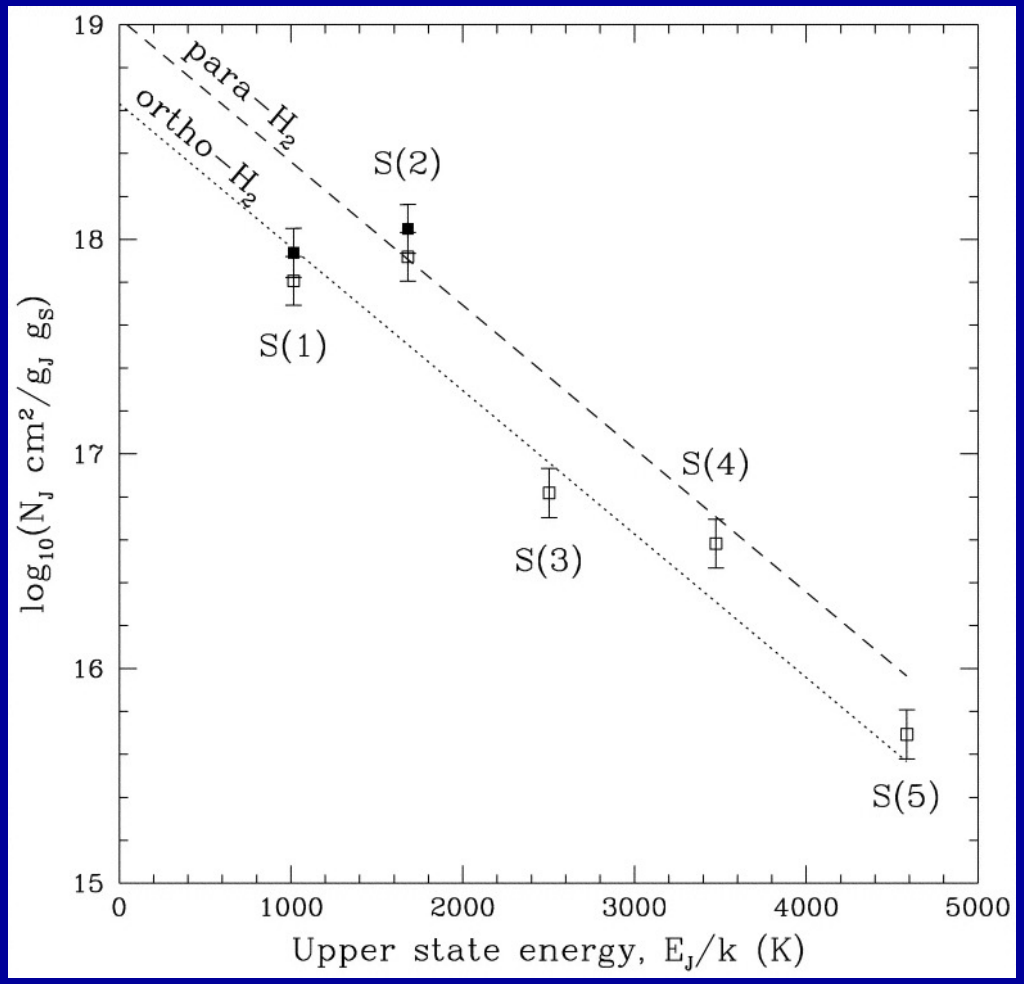

Shock heating suggested

- Shock waves heat gas temporarily: time spent hot is smaller than the ortho/para conversion time

- Compared results with predictions based on detailed calculations of Timmerman (1996, ApJ)
  - Para-to-ortho conversion is dominated by reactive collisions

    $p - H_2 + H \rightarrow H + o - H_2$

    (activation energy barrier $\Delta E_A/k \sim 4000$ K)

  - Ortho/para ratio in HH54 consistent with models for shocks with velocity 10 – 20 km/s

H_2 rotational diagrams for HH54 observed with Spitzer

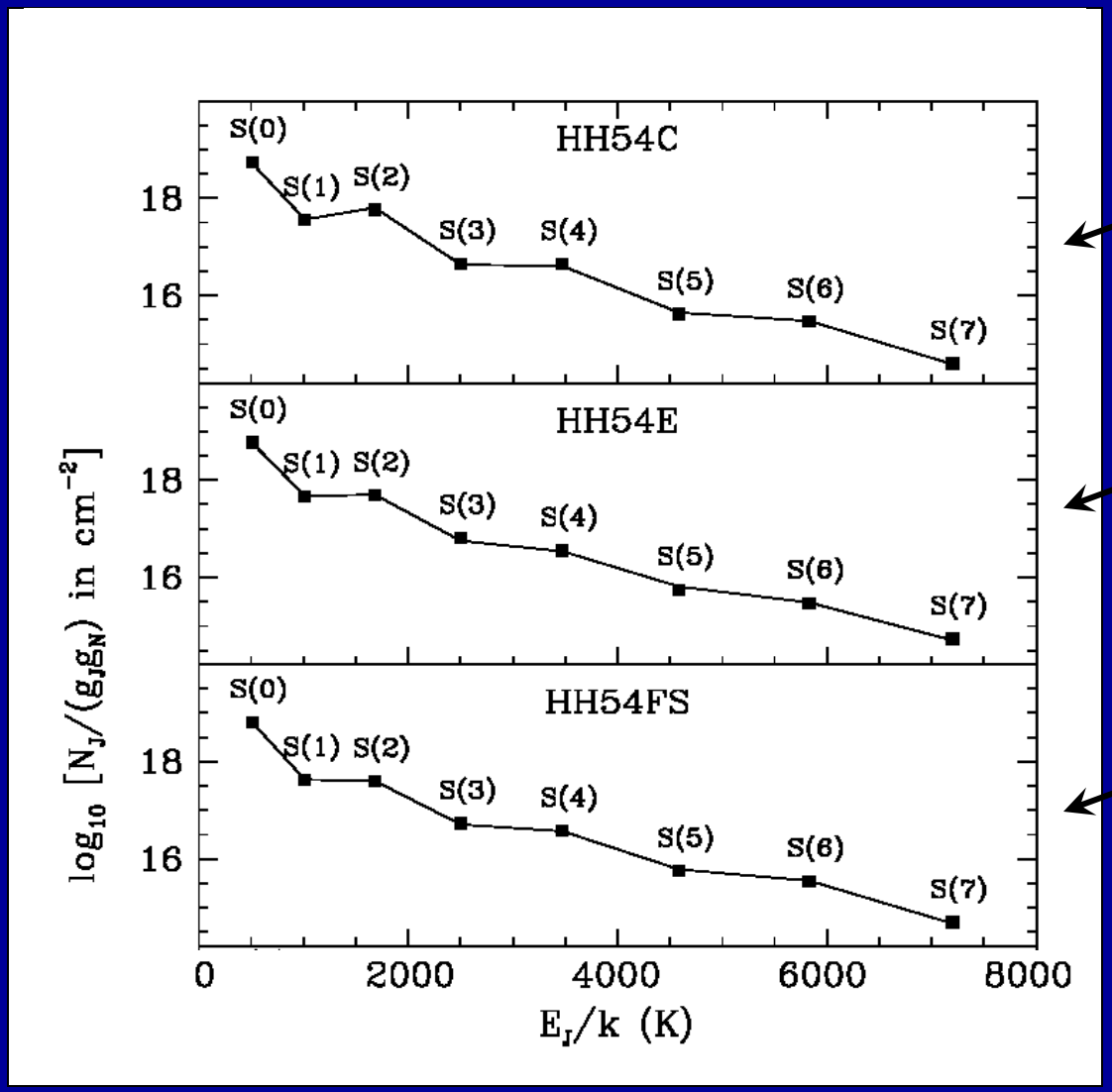

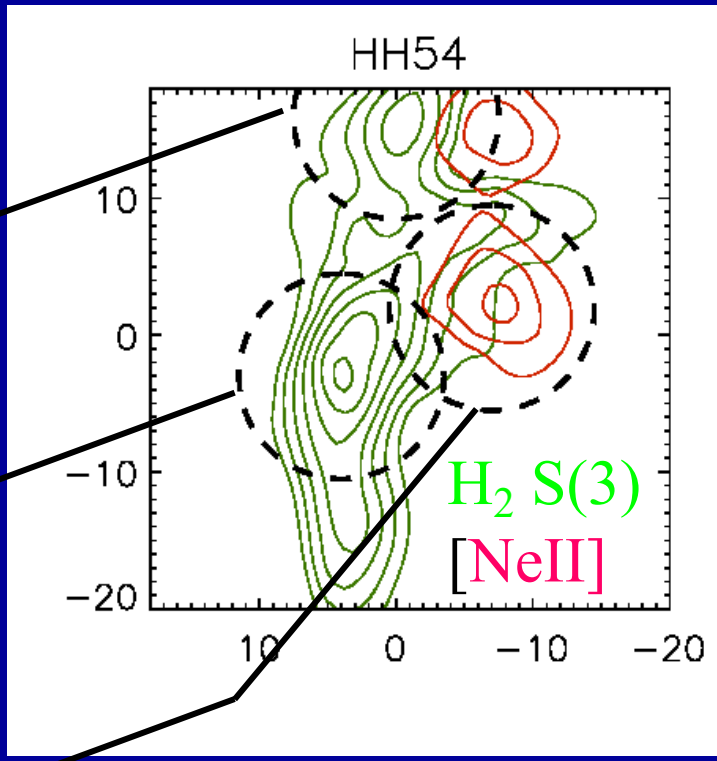

Fits to rotational diagrams

- Curvature → multiple temperatures present
  - We typically get good agreement with a two-component fit that invokes a warm component at $T_W \sim 400$ K and a hot component at $T_H \sim 1000$ K
  - Consistent with a mixture of shock velocities in the range 10 – 25 km/s
- Zigzag behavior
  - H_2 ortho-to-para ratio is smaller than 3
  - Compelling evidence for non-equilibrium chemistry
  - Departures from LTE are greater for the lower temperature components
  - Para → ortho conversion more efficient in faster, hotter shocks

Can we actually see this para → ortho conversion taking place within a shock?

The linear scale is ~ (0.001/n_4) pc ~ (1/n_4) arcsec at 200 pc, where the preshock density of H nuclei = 10^4 n_4 cm^{-3}

(Should be detectable with JWST)

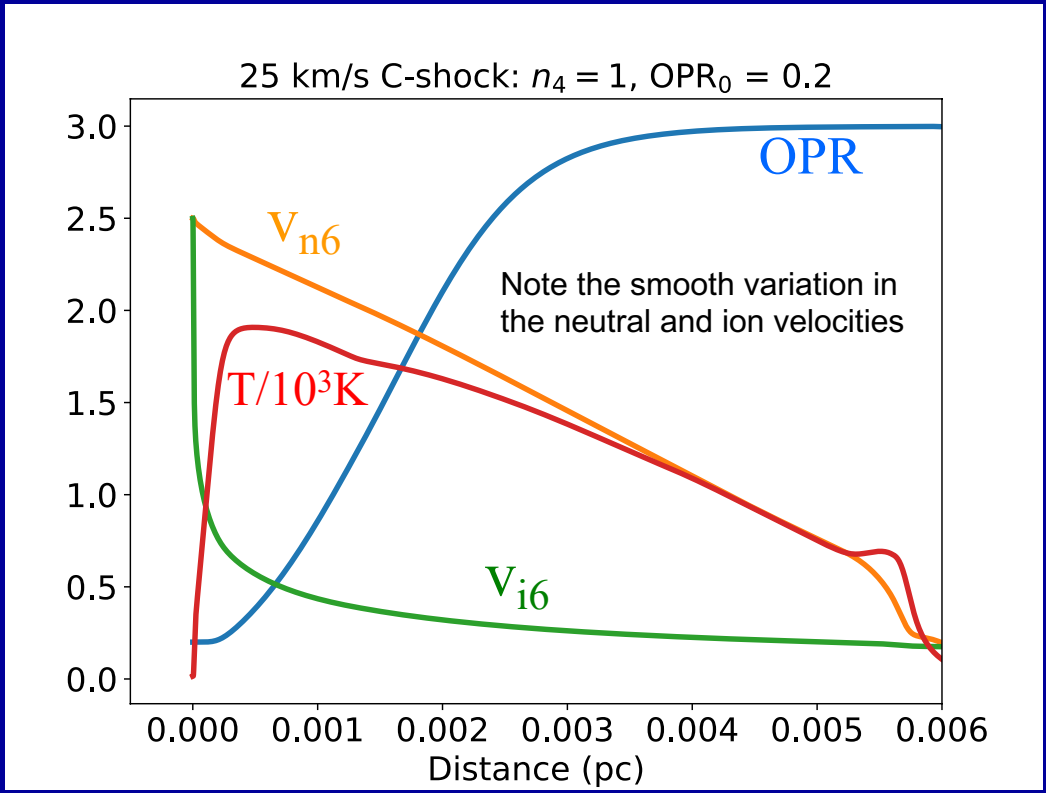

Pierre Lesaffre (Paris-Durham shock code)

Can we actually see this para → ortho conversion taking place within a shock?

But we might hope to see a frequency shift between the ortho- and para-H_2 lines

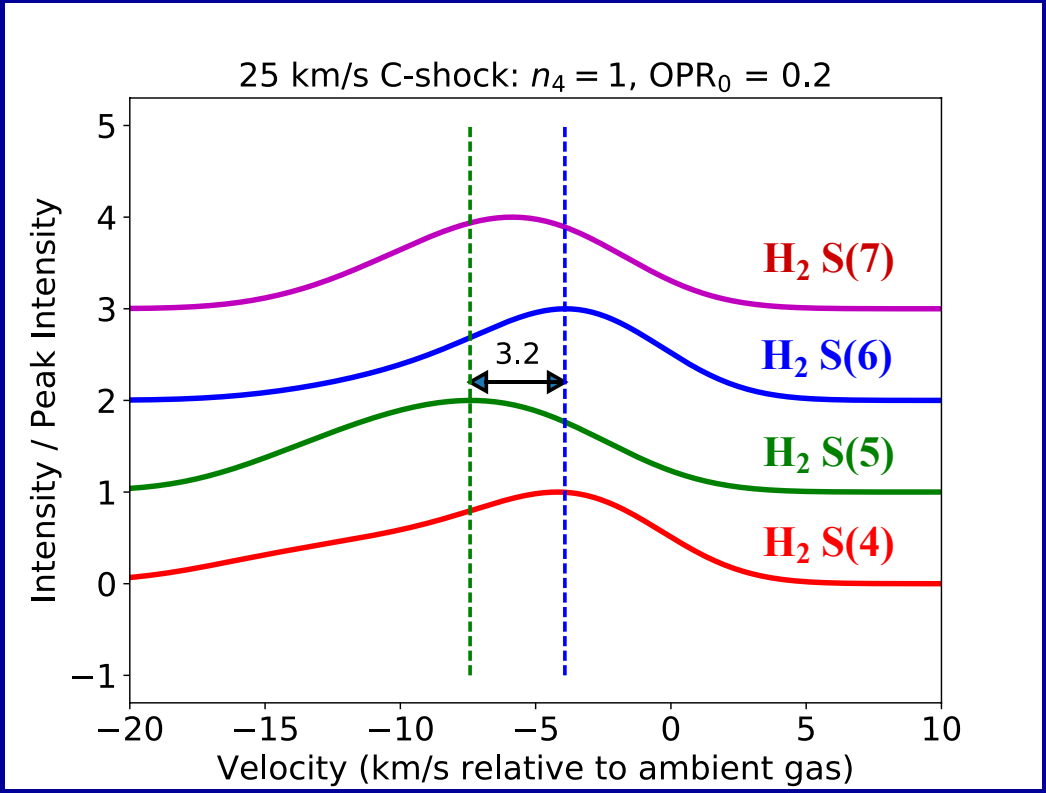

Pierre Lesaffre (Paris-Durham shock code)

EXES observations

Performed mid-Oct 2018 in Cycle 6 GO program

Total time: 10.5 hours spread over 4 flights

We observed four pure rotational emission lines of H_2

Two para-H_2 lines

S(4) (i.e. $J = 6 – 4$) at 8.2 μm

S(6) (i.e. $J = 8 – 6$) at 6.1 μm

Two ortho-H_2 lines

S(5) (i.e. $J = 7 – 5$) at 6.9 μm

S(7) (i.e. $J = 9 – 7$) at 5.5 μm

toward two positions in HH7

HH7: a bow shock driven by the jet from a YSO

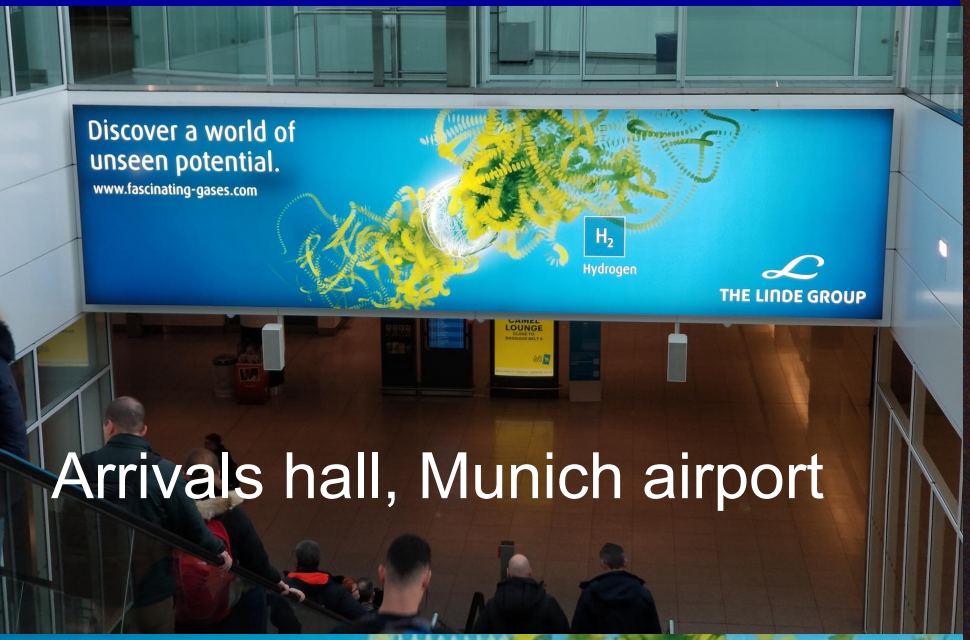

Arrivals hall, Munich airport

Credit: NASA/Hubble/Staplefeldt

SVS 13

HH 7

We used slit widths of 1.9 arcsec to achieve a spectral resolving power of 86,000

(equivalent to 3.5 km/s)

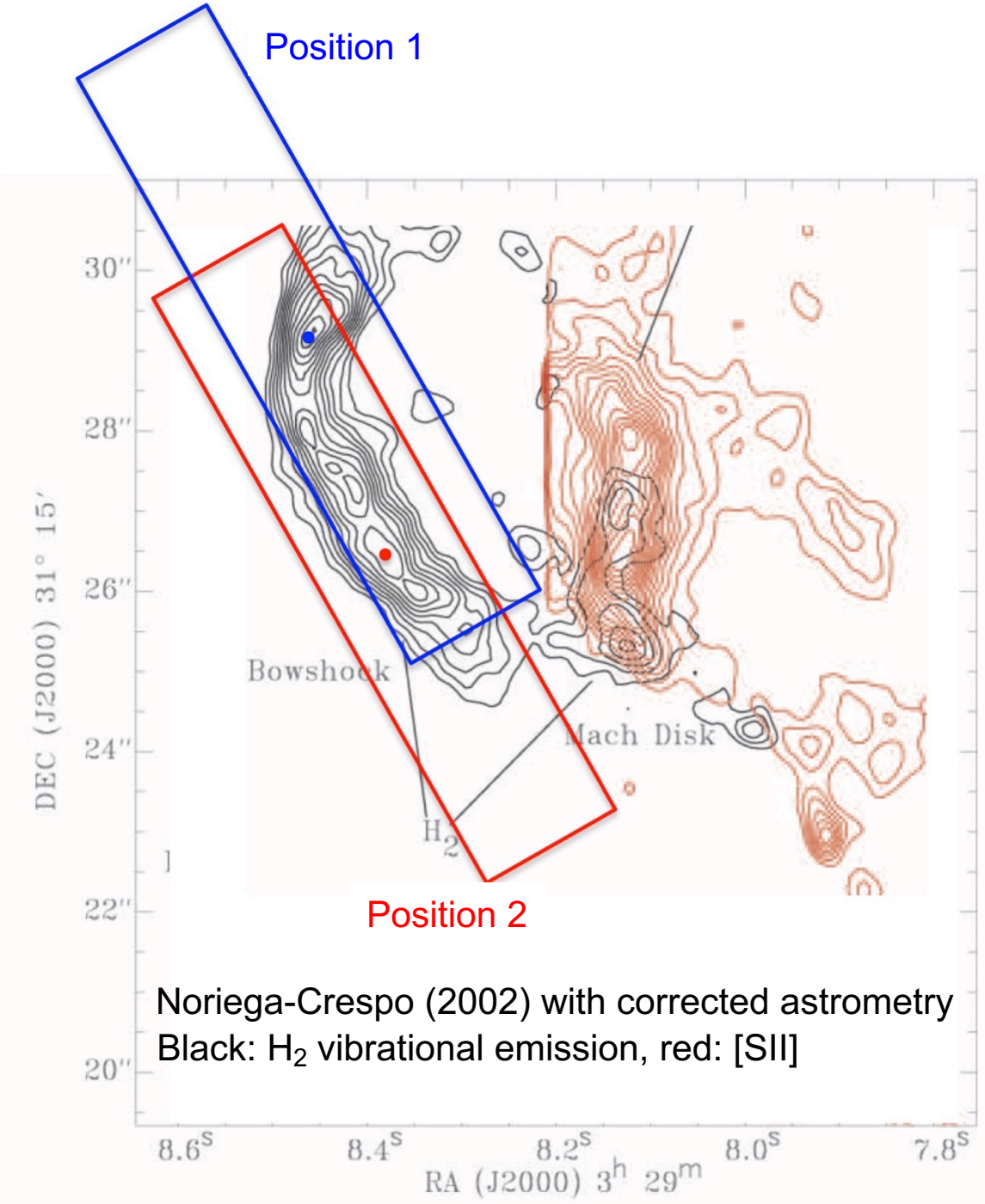

Noriega-Crespo (2002) with corrected astrometry
Black: H_2 vibrational emission, red: [SII]

Observed spectra

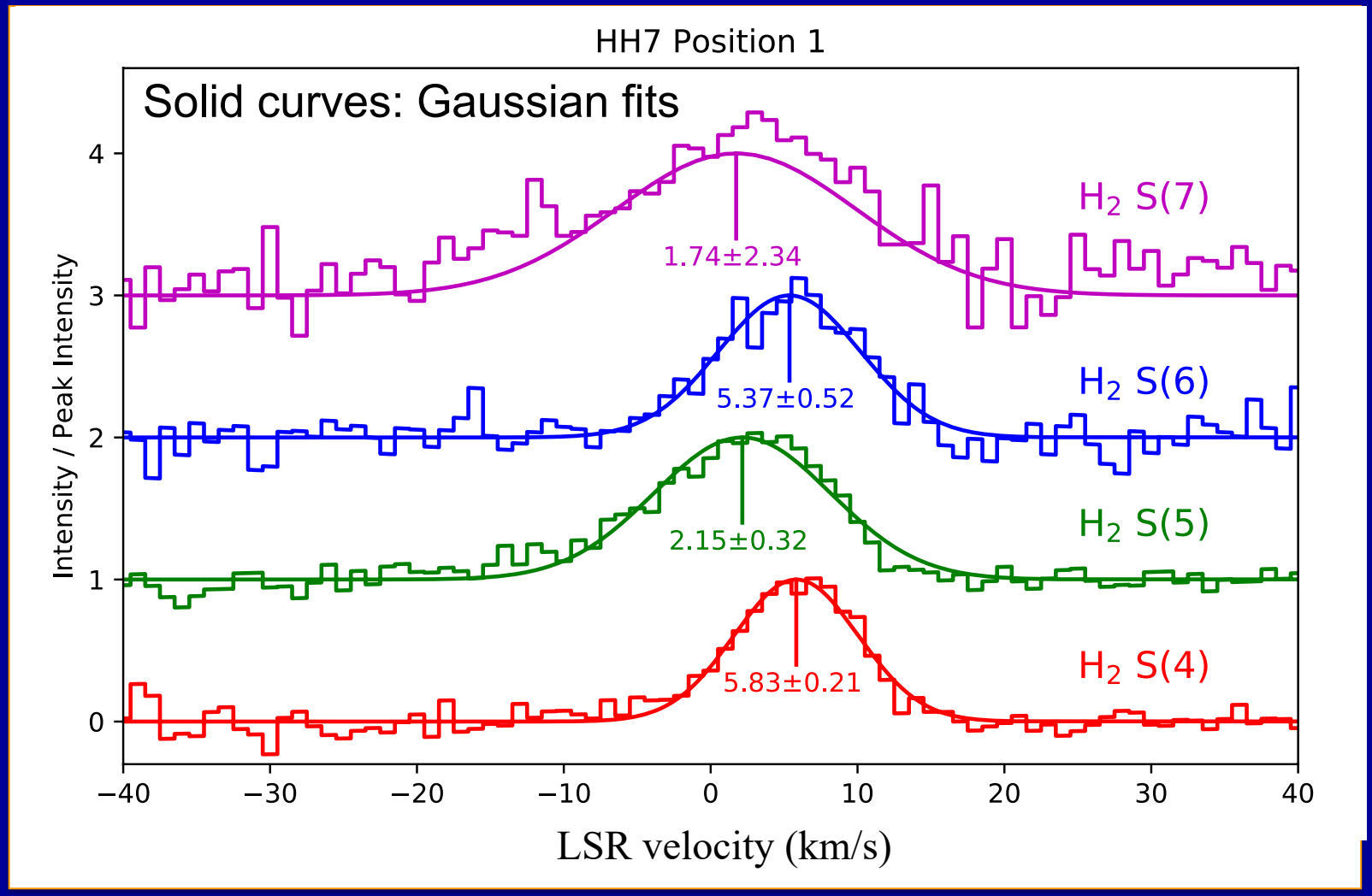

Clear evidence for an ortho-para shift of 3 – 4 km/s

Velocity centroid positions

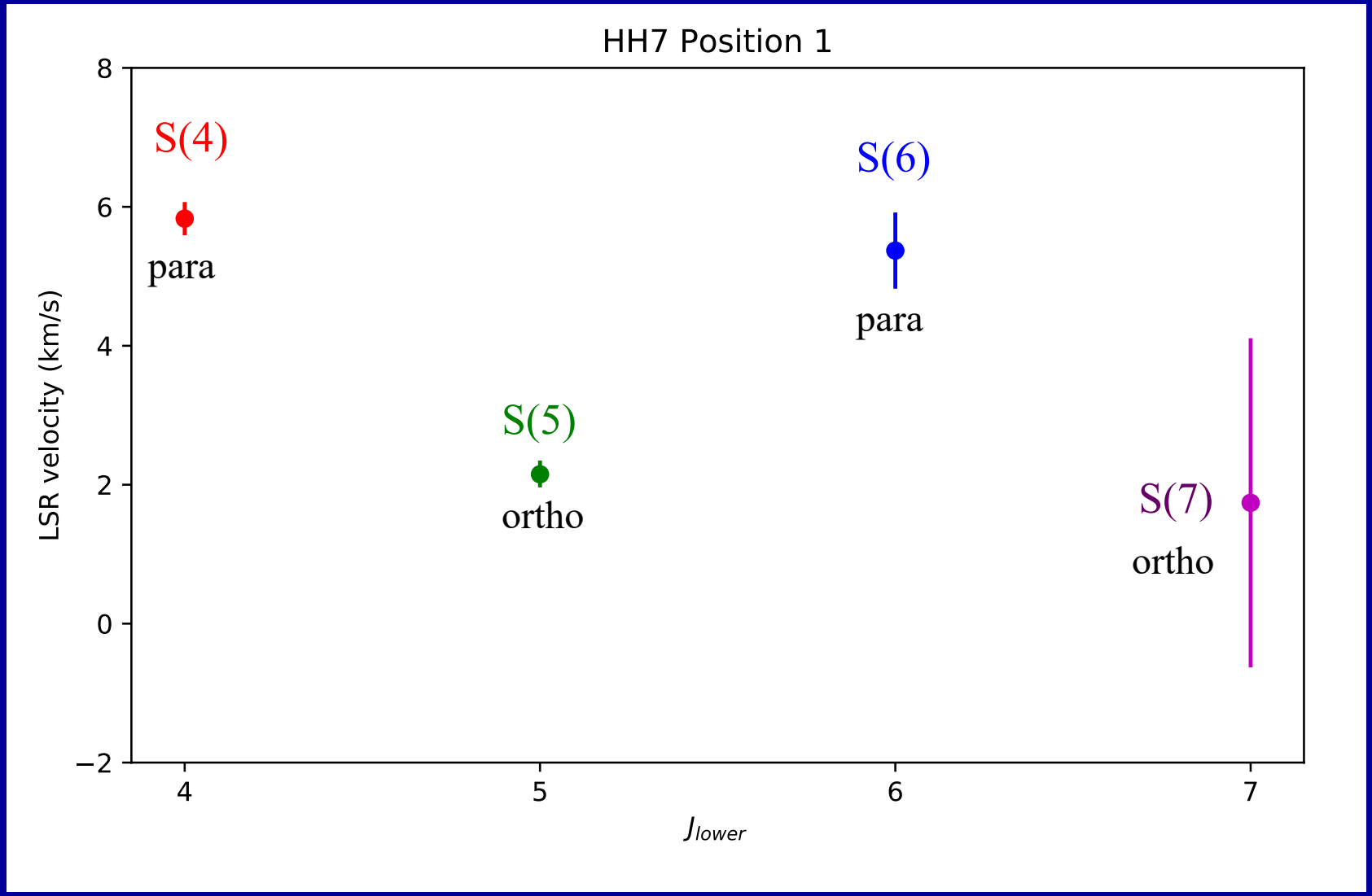

Relative strengths of S(4), S(5) and S(6) lines probe the ortho-to-para ratio and temperature

Can track para-ortho conversion through the shock

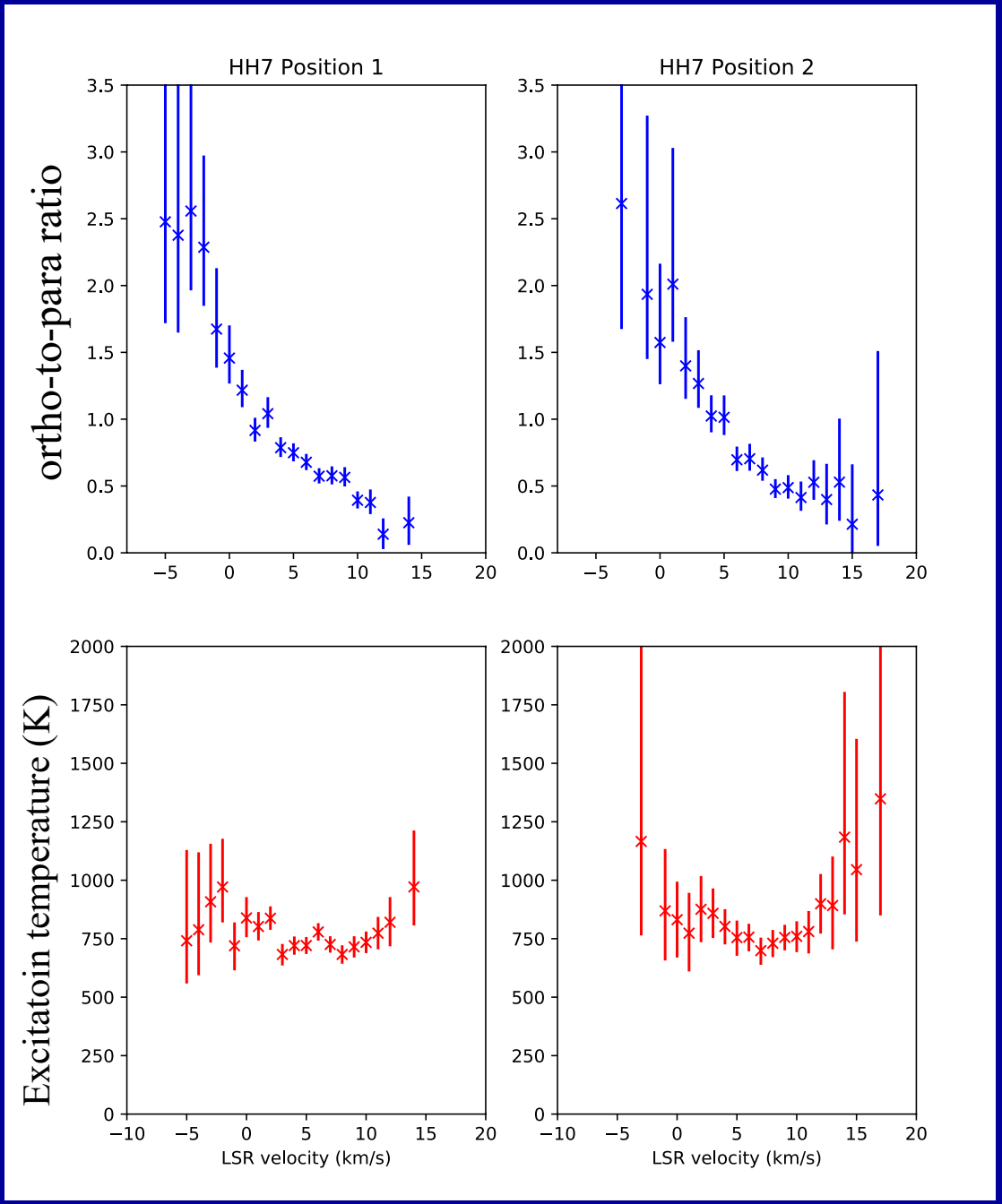

Summary of what we learn from the H_2 spectra obtained toward HH7

Zigzag rotational diagrams for the H_2 pure rotational lines observed from shocks provide the best example of interstellar chemistry that is out of equilibrium

With velocity-resolved observations, now possible for the first time with SOFIA/EXES, we can witness the return toward chemical equilibrium within the hot shocked gas and demonstrate that the flow velocity is changing during this process

The changing flow velocity is among the most direct evidence we have for ‘C’-type shocks in which the flow parameters vary continuously

H_2O vibrational absorption bands observed toward the massive protostar AFGL 2136

A combination of CRIRES and EXES spectra show more than 100 spectral features associated with water vapor.

There are roughly 70 unblended lines associated with absorption by water in the ground vibrational state. These originate in different rotational states within the ground vibration state and can be used to create a rotational diagram.

Most of the lines near 2.5 μm, observed with CRIRES, are in the $v_2 = 1 – 0$ and $v_3 = 1 – 0$ bands (stretching modes)

Most of the lines near 6 μm, observed with EXES, are in the $v_2 = 1 – 0$ bands (bending mode)

Four pure rotational transitions of H_2O, between 11.7 – 13.1 μm , are observed with TEXES

EXES spectra (Indriolo et al. 2020, ApJ)

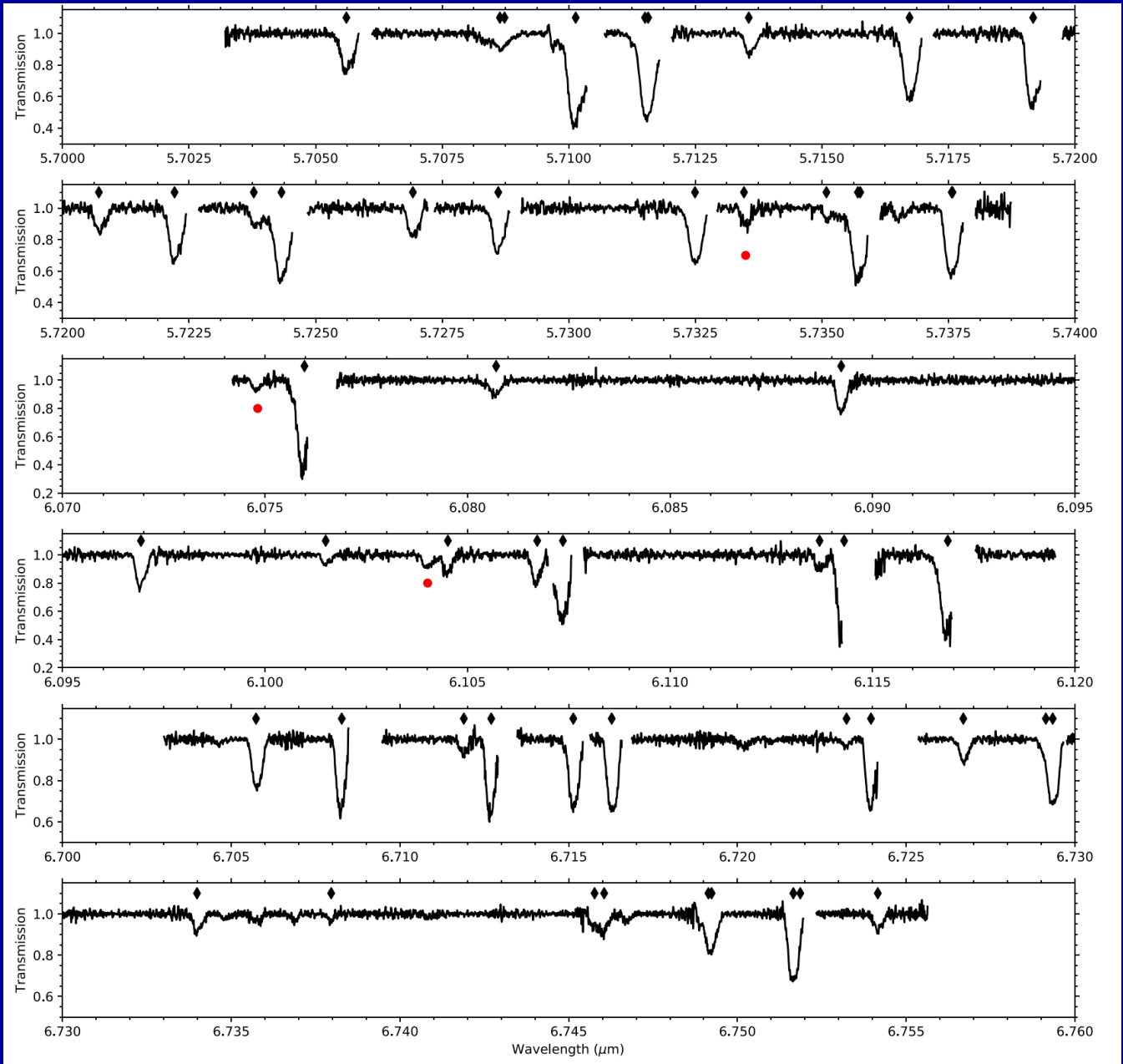

Rotational diagram

Column densities computed with the assumption that the absorption occurs in a foreground screen

Ortho-to-para ratio is consistent with 3

There is significant scatter, in which the deeper features imply lower than average column densities

May indicate that the dust that provides a background continuum is mixed in with the gas (contrary to the foreground screen model)

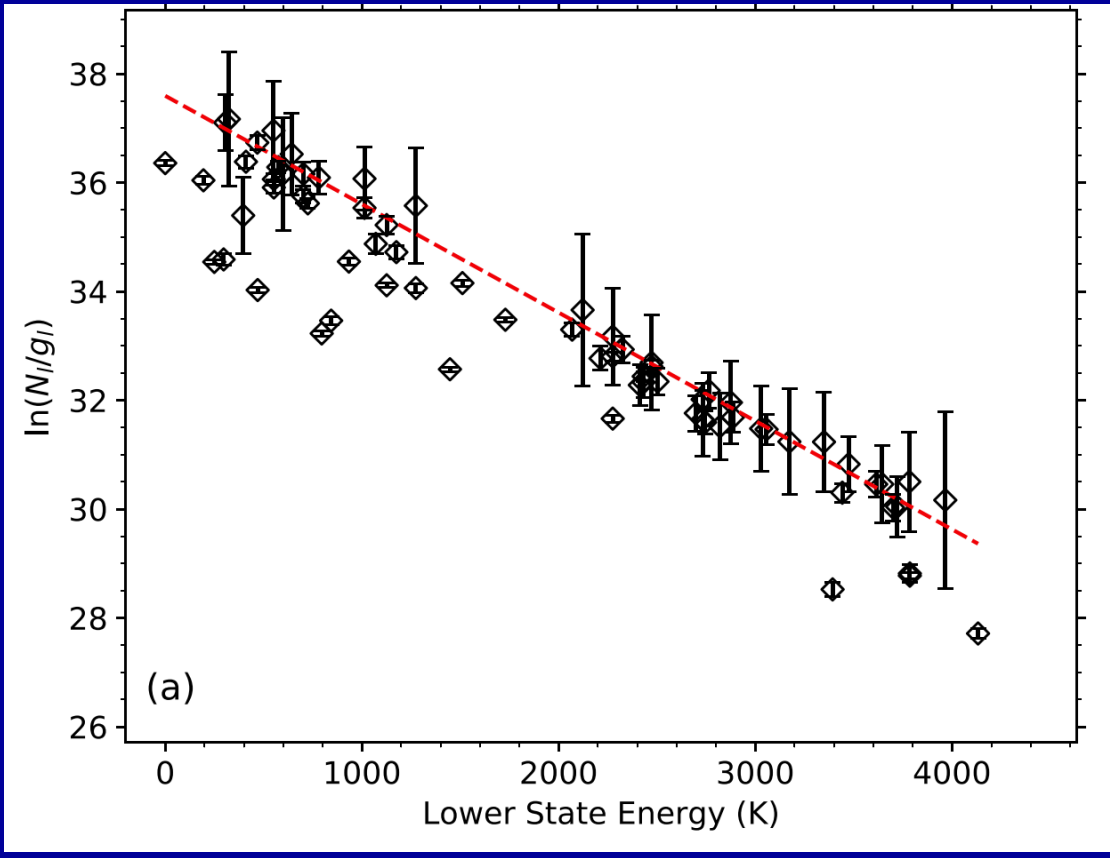

Derived column density and temperature

From the CRIRES data,

$N(H_2O) = 8.25 \pm 0.95 \times 10^{18}$ cm^{-2}

$T_{ex} = 502 \pm 12$ K

For comparison, CO vibrational spectra obtained by Goto et al. (2019) yield

$N(CO) = 2.8 \pm 0.4 \times 10^{19}$ cm^{-2}

$T_{ex} = 534 \pm 80$ K

Would imply $N(H_2O)/N(CO) \sim 0.3$ but there are uncertainties due to deficiencies in the foreground screen model

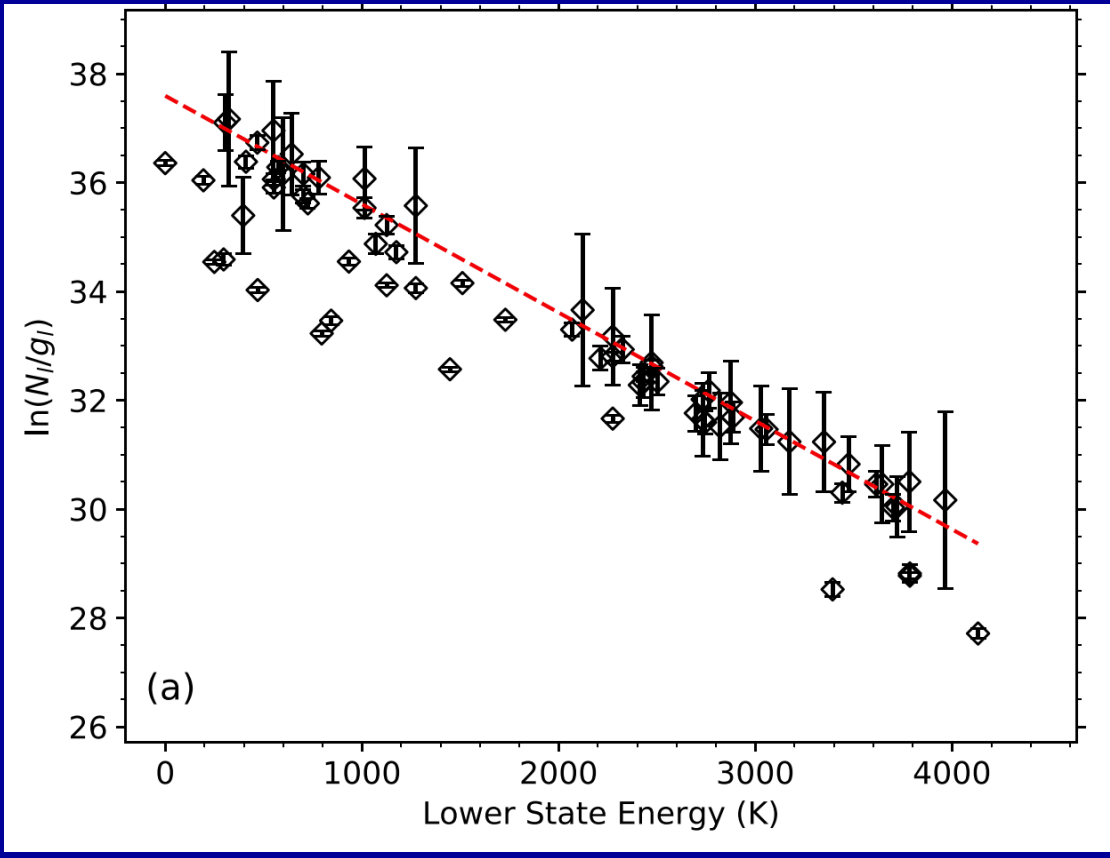

Many other molecules have also been detected by mid-IR observations toward this and similar sources

Barr et al. (2020, ApJ) used a stellar atmosphere theory approach to obtain abundances in an assumed disk (heated from the middle)

Table 3
Summary of Species in AFGL 2136

Species	Band	λ_0 (μm)	Number of Lines	Temperature (K)	N (cm^{-2})	Abundance (w.r.t. H)	v_{lsr} (km s^{-1})	ΔV (km s^{-1})
$C^{18}O$	v = 0–1	⋯	6	27 ± 2	$8.7 \pm 0.7 \times 10^{15}$	$2.8 \pm 0.1 \times 10^{-6}$	22.2 ± 0.3	2 ± 0.8
	v = 0–1	⋯	20	440 ± 15	$2.9 \pm 0.2 \times 10^{16}$	$1.9 \pm 0.1 \times 10^{-6}$	27.1 ± 0.6	12.3 ± 1.5
^{12}CO	v = 1–2	4.7	26	661 ± 9	$2.7 \pm 0.2 \times 10^{16}$	$1.7 \pm 0.4 \times 10^{-6}$	27.1 ± 0.3	12.1 ± 0.7
H_2O	ν_1/ν_3	2.5	34	[a]502 ± 12	[a]$8.25 \pm 0.95 \times 10^{18}$	⋯	24.6 ± 1.1	13.2 ± 2.5
HCN	ν_2 v$_2$ = 0–2	7.0	18	592 ± 21	$1.8 \pm 0.2 \times 10^{17}$	$1.6 \pm 0.8 \times 10^{-5}$	26.2 ± 0.5	8.5 ± 1.6
	ν_2 v$_2$ = 0–1	14.0	15	625 ± 19	$4.6 \pm 0.2 \times 10^{16}$	$5.3 \pm 0.4 \times 10^{-6}$	26.1 ± 0.5	11.0 ± 1.5
CS	v = 0–1	7.8	13	418 ± 23	$1.6 \pm 0.1 \times 10^{16}$	$1.2 \pm 0.1 \times 10^{-6}$	26.1 ± 0.4	8.0 ± 1.1
p-C_2H_2	ν_5	13.7	6	576 ± 61	$8.8 \pm 0.7 \times 10^{15}$	$1.0 \pm 0.4 \times 10^{-6}$	27.0 ± 0.3	10.9 ± 1.1
o-C_2H_2	ν_5	13.7	10	595 ± 23	$1.6 \pm 0.1 \times 10^{16}$	$1.7 \pm 0.1 \times 10^{-6}$	27.2 ± 0.3	11.3 ± 0.9
	$2\nu_5^2 - \nu_5^1$	13.7	10	480 ± 41	$1.6 \pm 1.0 \times 10^{15}$	$2.3 \pm 0.1 \times 10^{-7}$	26.6 ± 0.4	7.1 ± 1.2
	$(\nu_4 + \nu_5)^2 - \nu_4^1$	13.7	7	253 ± 30	$1.7 \pm 1.5 \times 10^{15}$	$1.3 \pm 1.3 \times 10^{-7}$	26.9 ± 0.6	8.1 ± 1.8
	$(\nu_4 + \nu_5)^0 - \nu_4^1$	13.7	6	692 ± 197	$2.1 \pm 0.2 \times 10^{15}$	$2.3 \pm 2.0 \times 10^{-7}$	26.8 ± 0.6	8.5 ± 1.9
	$(\nu_4 + \nu_5)$	7.5	12	618 ± 176	$5.0 \pm 0.1 \times 10^{16}$	$7.0 \pm 0.8 \times 10^{-6}$	26.0 ± 0.5	8.0 ± 1.5
p-NH_3	ν_2 v$_2$ = 0–1	9.5	32	435 ± 20	$1.0 \pm 0.5 \times 10^{16}$	$1.0 \pm 0.1 \times 10^{-6}$	28.1 ± 0.4	6.7 ± 1.0
o-NH_3	ν_2 v$_2$ = 0–1	9.5	17	493 ± 24	$0.9 \pm 0.4 \times 10^{15}$	$9.7 \pm 0.5 \times 10^{-7}$	27.7 ± 0.3	7.7 ± 0.9

Notes. No abundances relative to H are given for H_2O because stellar atmosphere theory is not used in the analysis of Indriolo et al. (2020).
[a] Indriolo et al. (2020).

Barr et al. (2022 , ApJ) obtained N(H_2O)/N(CO) ~ 1.6 using the same approach